# Soil-structure Interaction Effects on Tall Industrial Chimney Subjected to Along-wind Load

Sandeep G S, Arun Kumar Y M, Poornachandra Pandit and Jayalekshmi B R

Abstract—The present study focuses on the soil-structure interaction (SSI) effects on tall industrial chimneys subjected to along-wind loading. The influence of soil flexibility because of soil-structure interaction significantly affects the dynamic behavior and wind-induced vibrations of tall structures subjected to wind loads. A 3D finite element (FE) model has been developed to represent the integrated system comprising of chimney structure, annular raft foundation, and supporting soil. The model accounts for both self-weight and along-wind load, enabling a comprehensive assessment of the system's response. The analysis specifically aims to evaluate the vertical displacement of a raft, contact pressure distribution beneath the raft, bending moment distribution within annular raft foundation, and modal analysis of the chimney. Two different SSI approaches, the Winkler foundation model and the Elastic Continuum model (a more refined and realistic model), have been employed. Their results are compared with those from the conventional (non-interactive) method, which typically assumes a rigid base or ignores soil flexibility. The findings indicate that the inclusion of SSI, particularly using the Winkler and the Elastic Continuum approaches, leads to a notable reduction in bending moments in the raft foundation as compared to the conventional method. This reduction is attributed to the redistribution of stress and the flexibility of the supporting soil, which allows for a more realistic representation of how the foundation interacts with the underlying soil.

Index Terms—Tall industrial chimney; soil-structure interaction; contact pressure; vertical displacement; radial moment; tangential moment.

# I. INTRODUCTION

CHIMNEYS are symbolic of industrial growth and technological advancement, serving a vital role in managing air quality by dispersing toxic fumes at significant heights, thereby ensuring that pollutant concentrations at ground level remain within acceptable environmental limits

Manuscript received June 8, 2025; revised August 14, 2025.

Sandeep G S is an Assistant Professor of the Department of Civil Engineering, Manipal Institute of Technology, Manipal Academy of Higher Education, Manipal, 576104, India (e-mail: sandeep.gs@manipal.edu).

Arun Kumar Y M is an Assistant Professor of the Department of Civil Engineering, Manipal Institute of Technology, Manipal Academy of Higher Education, Manipal, 576104, India (corresponding author; phone: +91 9611842032; e-mail: kumar.arun@manipal.edu).

Poornachandra Pandit is an Associate Professor of the Department of Civil Engineering, Manipal Institute of Technology, Manipal Academy of Higher Education, Manipal, 576104, India (e-mail: pc.pandit@manipal.edu).

Jayalekshmi B R is a Professor of the Department of Civil Engineering, National Institute of Technology Karnataka (NITK), Surathkal, Karnataka, 575025, India (e-mail: brjaya@nitk.edu.in).

[1]-[7]. As environmental regulations have become stringent in recent years and industries have expanded, the height of chimneys has increased over the decades to improve the dispersion of pollutants and reduce their impact on surrounding areas. This trend towards constructing taller chimneys is expected to continue due to the growing emphasis on pollution control and the need to meet regulatory requirements. However, as chimney height increases, these slender structures become increasingly susceptible to lateral forces, particularly wind and seismic loads [8]-[13]. Their dynamic response to such loads becomes a critical consideration in both design and analysis. From a structural perspective, chimneys are typically designed with a hollow circular cross-section, which offers aerodynamic advantages by minimizing wind resistance and vortex-shedding effects. Additionally, the tapered elevation profile of chimneys that are wider at the base and narrower at the top not only enhances their aerodynamic performance but also contributes to material efficiency and structural economy, reducing the overall weight and construction costs while maintaining adequate strength and stability.

In most conventional civil engineering analyses, structures are often assumed to be fixed at their bases, simplifying the modeling and design process. However, the behavior of a structure is significantly influenced by the stiffness of the supporting soil, which can alter the way loads are distributed and resisted by the structural system. This deviation from idealized assumptions becomes especially important when considering SSI effects. For many ordinary structures, such as low-rise buildings or rigid retaining walls constructed on relatively stiff soils, neglecting SSI effects is generally acceptable and does not significantly compromise accuracy. In such cases, the foundation movement is minimal, and the structural response can be reasonably predicted using fixed-base models. However, the importance of considering SSI becomes critical for large and heavy structures founded on soft or medium-stiff soils [12]-[15]. Examples include nuclear power plants, cooling towers, high-rise buildings, and tall industrial chimneys. These structures impose substantial loads on their foundations and are sensitive to ground movement, making them more prone to foundation flexibility and differential settlement. Ignoring SSI in these cases may lead to inaccurate estimation of internal forces, unsafe design, or excessive conservatism. To understand the influence of soil flexibility on the dynamic behavior of a structure, a modal analysis of the SSI system is first conducted. This initial step is crucial in identifying how the presence of a flexible supporting medium, such as soil, affects the natural frequencies of the structure. Unlike fixed base models, which assume a rigid foundation, SSI models account for the deformable nature of the ground, thereby providing a more realistic representation of structural response [16]-[17]. One of the key impacts of SSI is the alteration in the pressure distribution between the foundation and the soil. For massive structures like industrial chimneys, an accurate evaluation of this contact pressure is essential for the design of an annular raft or mat foundation. Relying on simplified or conventional approaches may not capture the true interaction behavior. To address this, finite element methods (FEM) offer a robust and reliable tool for simulating the complex interactions between soil and structure [3], [14]. By modeling the chimney, its foundation, and the surrounding soil as an integrated system, FEM allows for a more realistic representation of load transfer, pressure distribution, and overall structural performance. This leads to better-informed design decisions, improved safety margins, and potentially more economical foundation systems.

#### II. METHODOLOGY

Industrial chimneys are constructed at a wide range of heights, from relatively low-rise structures to towering installations exceeding 300m. As chimney height increases, the choice of construction material becomes crucial from both structural and economic perspectives. For very tall chimneys, reinforced cement concrete (RCC) is generally preferred over steel due to its greater stiffness, durability, particularly cost-effectiveness, environmental and dynamic loads over long periods. In the present study, the focus is placed on assessing the influence of SSI on tall industrial chimneys subjected to along-wind loading. To understand how soil type affects the overall response of the chimney system, the investigation incorporates various soil conditions, representing different levels of soil stiffness. To capture the role of structural geometry, the study also examines chimneys with different slenderness ratios, which are defined as the ratio of height (H) to the base diameter (D<sub>b</sub>). In the present study, 400m tall chimneys with slenderness ratios of 7, 12, and 17 have been considered [18]-[20]. These values represent a range from relatively stocky to highly slender chimneys, each exhibiting distinct dynamic behavior and interaction characteristics with the supporting soil. The geometrical properties of the chimney shell and annular raft are tabulated in Table I.

In the present study, the foundation conditions for tall industrial chimneys are modeled by considering a range of soil types, specifically from loose soil to very dense soil, to evaluate the effects of soil stiffness on structural behavior under along-wind loading. The soil is represented using two widely adopted methods: the Winkler Spring model and the Elastic Continuum approach. In the Winkler Spring model, the soil is idealized as a series of discrete, independent springs. The spring stiffness at each location on the raft foundation is determined based on the modulus of subgrade reaction ( $K_s$ ), which reflects the stiffness of the supporting soil beneath each contact point [21]-[25]. Importantly, the spring stiffness is also dependent on the contact area of the

individual spring element within the raft mesh, making it sensitive to the spatial variation in load distribution. Alternatively, the Elastic Continuum model provides a more realistic representation of soil behavior by considering it as a continuous elastic medium [26]. In this method, the soil response is governed by two primary parameters: the elastic modulus of the soil (Es) and its unit weight ( $\gamma_s$ ). For the present study, the unit weight of soil is assumed as  $18kN/m^3$ , which is typical for granular soils like sand. The moduli of subgrade reactions of the range of soils considered in the present study are tabulated in Table II.

In the current study, the along-wind load acting on tall industrial chimneys has been computed in accordance with the guidelines provided in IS: 4998 (Part 1) [27], which deals specifically with the structural design criteria for reinforced concrete chimneys under wind loads. The chimneys considered in the analysis are classified as Class C structures, a designation that accounts for their importance and expected performance during their service life. The terrain category selected for the study is Category 2, as per IS: 875 (Part 3) [28]. This terrain type typically represents areas with low-rise obstructions, such as open terrain with scattered buildings, which moderately influence the wind flow profile around tall structures like chimneys. A basic wind speed of 50m/s is assumed uniformly for all chimneys considered in the present study. This speed corresponds to a high wind zone and represents severe wind loading conditions, ensuring that the design and analysis are conservative and applicable to demanding real-world scenarios.

TABLE II  $\mbox{MODULUS OF SUBGRADE REACTION OF SOIL } (K_s)$ 

| Type of soil      | Modulus of subgrade reaction of soil (kN/m³) |  |  |  |
|-------------------|--|--|--|--|
| Loose Soil        | 10×10 <sup>3</sup>                           |  |  |  |
| Medium-Dense Soil | 40×10 <sup>3</sup>                           |  |  |  |
| Dense Soil        | 100×10 <sup>3</sup>                          |  |  |  |
| Very Dense Soil   | 1×10 <sup>16</sup>                           |  |  |  |

The along-wind load analysis is conducted by considering SSI effects for chimneys with varying geometric parameters, particularly different slenderness ratios, and soil types. The analysis includes multiple support conditions, modeled using both Winkler Spring and Elastic Continuum approaches, to reflect a range of realistic foundation behaviors. The results obtained from the SSI-based finite element analysis are systematically compared with those from the conventional fixed-base method, which typically neglects the flexibility of the soil. This comparative evaluation highlights the influence of SSI on critical response parameters such as base moments, displacement profiles, and contact pressure distributions.

#### A. Idealization of Chimney Structure

In the present study, the structural modeling of the chimney and its annular foundation has been carried out using SHELL63 element, a four-node elastic shell element available in ANSYS software [29]-[32]. This element is particularly suitable for analyzing thin to moderately thick shell structures, as it offers both bending and membrane capabilities, allowing for accurate simulation of the

chimney's response to wind loads. Each node of the SHELL63 element possesses six degrees of freedom, three translational degrees of freedom (in x, y, and z directions), and three rotational degrees of freedom (about x, y, and z axes). This comprehensive degree of freedom configuration enables the element to effectively capture complex stress distributions and deformations within the structure. The chimney shell has been discretized with a vertical element size of 2m, ensuring sufficient resolution along the height to capture the structural behavior under wind loading. In the circumferential direction, the model includes 150 divisions, providing a fine mesh to accurately simulate the circular geometry and the associated aerodynamic and structural responses. Similarly, the annular foundation raft has been modeled using the same SHELL63 element. It is discretized with 2m divisions in the radial direction and 150 divisions circumferentially, ensuring consistency with the chimney mesh and maintaining numerical accuracy at the interface between the chimney and the foundation. The chimney and foundation are assumed to be monolithically constructed using RCC of grade M30. Both components are modeled as elastic, which is a reasonable assumption for serviceability level analysis under wind loads. The material properties used for the chimney shell and annular raft are tabulated in Table III.

 $\label{thm:constraint} TABLE\,III$  Properties of the chimney shell and annular raft

| Parameter                            | Chimney shell        | Annular raft          |
|--------------------------------------|----------------------|-----------------------|
| Unit weight (kN/m <sup>3</sup> )     | 25                   | 25                    |
| Young's modulus (kN/m <sup>2</sup> ) | 33.5×10 <sup>6</sup> | 27.39×10 <sup>6</sup> |
| Poison's ratio                       | 0.2                  | 0.2                   |

### B. Idealization of Soil

In the static SSI analysis, two widely adopted approaches for modeling supporting soil are the Winkler Spring model and the Elastic Continuum model, each offering distinct advantages based on the level of complexity and accuracy required.

# Winkler Spring model (Discrete Spring model)

In the Winkler Spring model, the soil medium is idealized as a series of independent, linearly elastic springs, which respond to vertical displacements only. This model is computationally efficient and suitable for preliminary or simplified analyses. In the current study, COMBIN14 elements are employed to represent these linear springs [33]-[35]. COMBIN14 is a spring-damper element with no mass and no bending or torsional capabilities, making it suitable for modeling vertical spring stiffness without additional complexities. The spring stiffness values are calculated based on Ks and the area of influence corresponding to each spring location. This approach assumes no interaction between adjacent springs and does not account for shear transfer within the soil mass, limiting its ability to capture complex deformation patterns. Fig. 1 shows the chimney shell and annular raft on a Winkler Spring model.

# Elastic continuum model (Finite element model)

To overcome the limitations of the Winkler Spring approach, the Elastic Continuum model provides a more

comprehensive representation of the soil mass by treating it as a continuous elastic body. In the present study, the SOLID45 element is used for this purpose [36]-[37]. SOLID45 is an 8-node element designed for 3D modeling of solid structures, with each node having three translational degrees of freedom in the x, y, and z directions. This method captures both vertical and lateral interactions and is suitable for modeling realistic soil deformation patterns under loading. The geometry of the soil model is defined to ensure sufficient domain size for realistic stress distribution. The lateral extents of the soil block are taken as four times the breadth of the foundation in all horizontal directions. The depth of the soil is taken as six times the breadth of the foundation. The soil side surfaces are restrained against movement in the lateral x and y directions. The bottom surface is fully restrained (all degrees of freedom are fixed) to simulate firm base support and eliminate rigid body motion. Fig. 2 shows the chimney shell and annular raft on a 3D Elastic Continuum model of the soil.

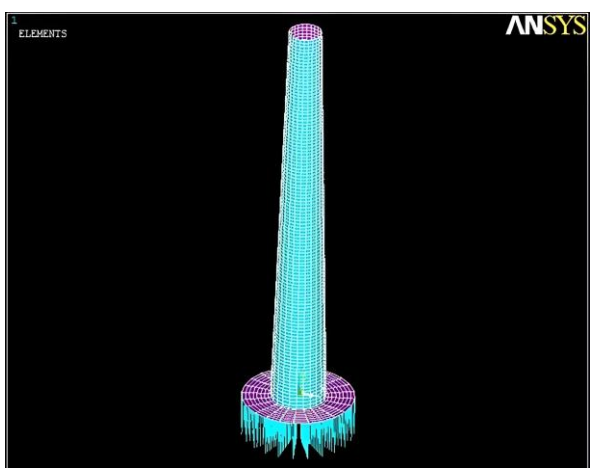


Fig. 1. Chimney shell and annular raft on a Winkler Spring model

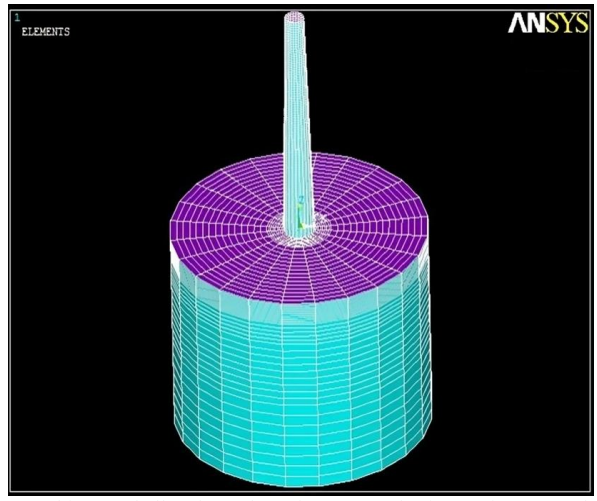


Fig. 2. Chimney shell and annular raft on a 3D Elastic Continuum model of soil

By employing both the Winkler Spring model and the continuum approach, the study offers a comprehensive evaluation of soil structure interaction. The use of these two distinct methods allows for a expressive comparison between simplified and detailed modeling techniques. While the Winkler approach provides a straightforward representation of soil behavior through an array of independent springs, the continuum method captures the

more complex and realistic deformation characteristics of the soil mass as a whole.

# III. RESULTS AND DISCUSSION

A. Variation in the vertical displacement of Chimney raft by Winkler Spring model approach

The vertical displacement pattern observed in the analysis highlights a non-uniform deformation of the raft foundation under the influence of along-wind loads, primarily due to soil-structure interaction effects and varying soil stiffness. For soft soil, particularly those with low subgrade stiffness, loose sand with  $K_s=10\times10^3 \text{ kN/m}^3$ , the raft exhibits significant differential settlement. The maximum downward displacement occurs under the windshield location on the leeward side of the chimney. This is due to asymmetrical pressure distribution caused by wind-induced moments and eccentric loading. On the windward side, the settlement pattern is relatively linear, with the maximum displacement occurring at the innermost edge of the raft, indicating the rotational behavior of the entire system about the center. For medium dense and dense sands with K<sub>s</sub>=40×10<sup>3</sup> to 100×10<sup>3</sup> kN/m<sup>3</sup>, the displacement profile becomes more uniform, with linear variation on both windward and leeward sides. This suggests a more balanced load transfer and reduces differential settlement, enhancing the stability of the structure. In case of very dense soil (with extremely

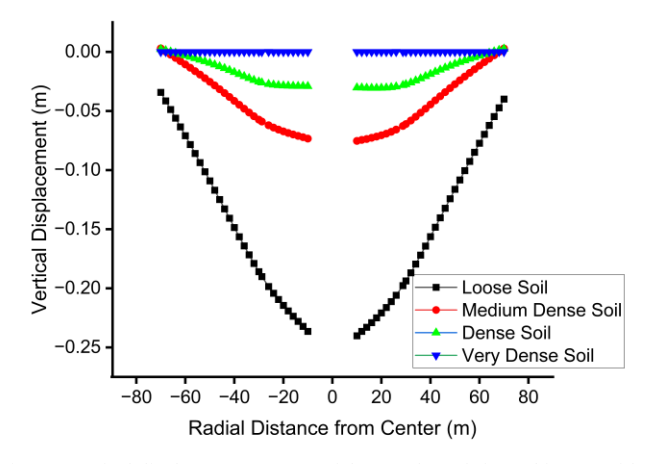


Fig. 3. Vertical displacement pattern of the annular raft for a chimney with  $H/D_b=7$  and  $D_0/t=12.5$ 

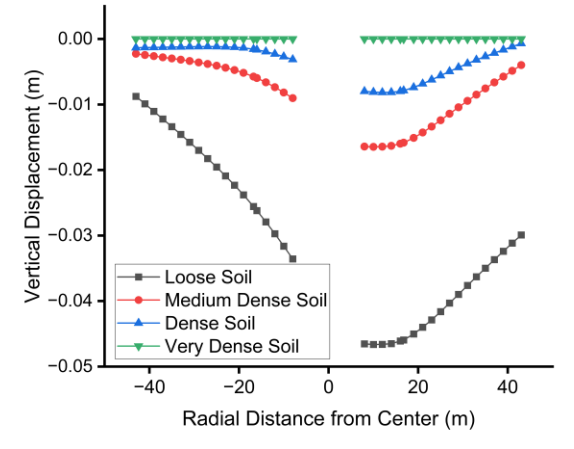


Fig. 4. Vertical displacement pattern of the annular raft for a chimney with  $H/D_b=12$  and  $D_0/t=12.5$ 

high stiffness, such as  $K_s = 1 \times 10^{16} \, kN/m^3$ , the foundation experiences negligible or zero displacement across the raft surface. The soil acts as a rigid support, preventing any visible settlement and minimizing structural deformations. Additionally, it is noted that, for chimneys with higher slenderness ratios, the windward side of the raft exhibits upward displacement. This is attributed to the overturning moment generated by wind loads, which causes an uplift force on the windward edge, particularly when supported on stiffer soils.

Fig. 3 presents the vertical displacement pattern of the annular raft subjected to along-wind load for a chimney with a slenderness ratio, H/D<sub>b</sub>=7 and outer diameter of raft to its thickness ratio,  $D_0/t=12.5$ . The displacement profile exhibits a symmetrical pattern on both windward and leeward sides, indicating a balanced deformation response around the chimney axis under wind loading. A key observation from the analysis is the inverse relationship between soil stiffness and raft displacement. As the soil stiffness increases, vertical displacement of the raft decreases significantly, due to the enhanced support from the stiffer soil medium. The maximum displacement occurs near the central windshield location, which experiences the highest concentration of load from wind-induced forces. In contrast, the outer edges of the raft experience the least displacement, reflecting the distribution of bending and support reactions. Quantitatively, the displacement behavior under varying soil conditions reveals the following: In medium-dense soil, the raft displacement reduces by approximately 64% compared to the soft soil condition. In dense soil, the displacement reduction is even more significant, by about 95% when compared to loose soil. These findings demonstrate the critical role of soil stiffness in controlling vertical displacement and overall foundation behavior. Incorporating SSI in the analysis leads to more realistic estimations of raft performance under lateral loading conditions, thereby ensuring better design accuracy and structural safety for tall chimneys.

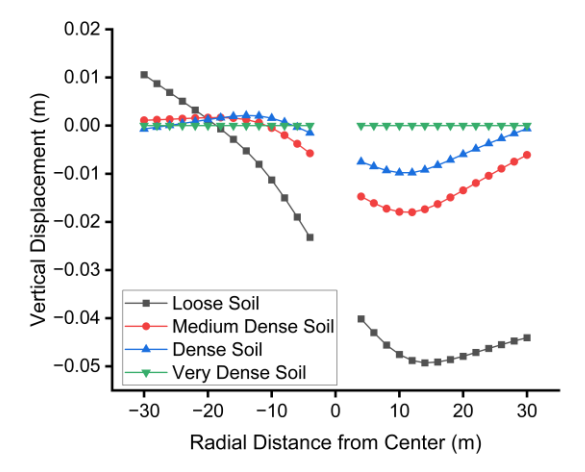


Fig.5 Vertical displacement pattern of the annular raft for a chimney with  $H/D_b=17$  and  $D_0/t=12.5$ 

Fig. 4 illustrates the vertical displacement pattern of the annular raft under along-wind loading for a chimney with a slenderness ratio,  $H/D_b=12$  and outer diameter of raft to its thickness ratio,  $D_0/t=12.5$ . While the displacement profile on the leeward side is similar to that observed in the

chimney with a slenderness ratio of 7, the windward side exhibits an inverted trend. This change is attributed to the increased height of the chimney, which results in a greater wind force absorption. For loose soil conditions, a non-zero displacement is observed at the outer edge of the raft. In medium-dense soil, the raft displacement decreases by approximately 200% compared to the soft soil condition. In dense soil, the reduction in displacement is even more pronounced, around 400%, when compared to the loose soil.

Fig. 5 illustrates the vertical displacement pattern of the annular raft under along-wind loading for a chimney with a slenderness ratio,  $H/D_b=17$  and outer diameter of raft to its thickness ratio,  $D_0/t=12.5$ . While the displacement profile on the leeward side is similar to that observed in the chimney with a slenderness ratio of 12, the windward side exhibits an inverted trend and extends towards a negative side. This change is attributed to the increased height of the chimney, which results in greater wind force absorption. For loose soil conditions, a non-zero displacement is observed at the outer edge of the raft. In medium-dense soil, the raft displacement decreases by approximately 300% compared to the soft soil condition. In dense soil, the reduction in the displacement is even more pronounced, which is around 400% when compared to the loose soil.

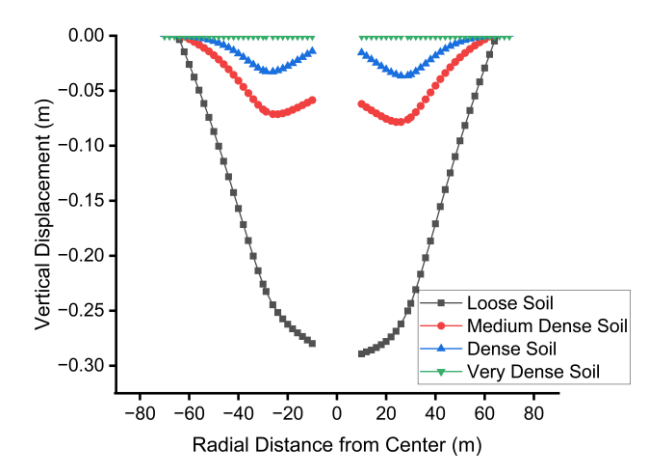


Fig.6 Vertical displacement pattern of the annular raft for a chimney with  $H/D_b=7$  and  $D_0/t=22.5$ 

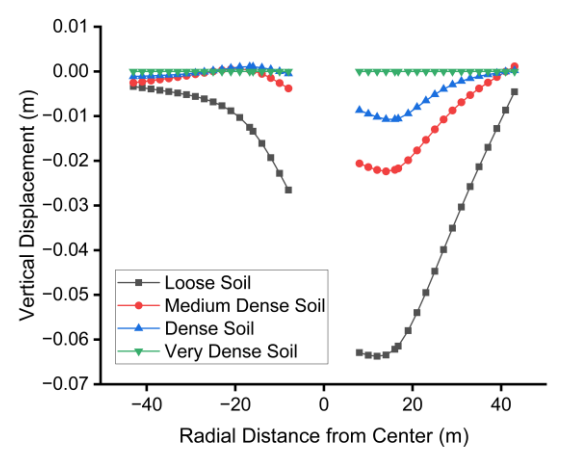


Fig.7 Vertical displacement pattern of the annular raft for a chimney with  $H/D_b=12$  and  $D_0/t=22.5$ 

It is evident from Fig 6, 7, and 8 that the vertical displacement of a chimney is higher across all slenderness

ratios when the raft thickness corresponds to a  $D_0/t$  ratio of 22.5 as compared to  $D_0/t$  ratio of 12.5. This behavior indicates that a relatively thinner raft offers reduced stiffness, allowing greater settlement under the load of a chimney shell.

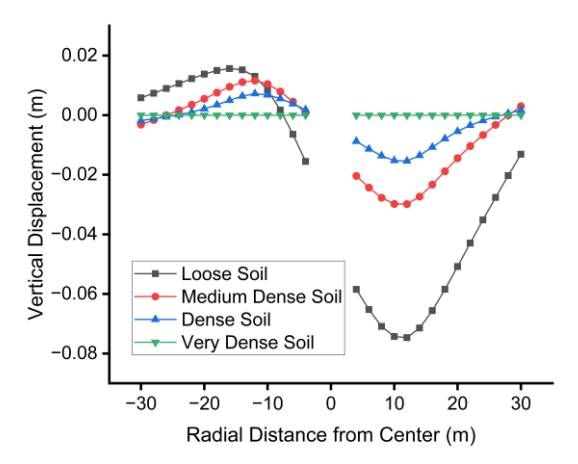


Fig.8 Vertical displacement pattern of the annular raft for a chimney with  $H/D_b=17$  and  $D_0/t=22.5$ 

Conversely, when  $D_0/t$  ratio increases to 22.5, the raft thickness decreases further, which in turn intensifies the pressure exerted by a chimney shell onto the raft. This increased load concentration not only heightens vertical displacement but can also influence the overall stress distribution within the foundation system, potentially affecting its long-term performance and service life.

# B. Variation of the contact pressure under Chimney raft by the Elastic Continuum model approach

In the conventional method of analysis, the foundation is idealized as rigid, implying that it has sufficient stiffness to distribute applied loads uniformly across the soil. This simplification assumes even contact pressure beneath the entire raft, which does not reflect the actual behavior of the soil-structure system under realistic loading conditions. In contrast, while using the SSI method, the contact pressure distribution becomes non-uniform, and its pattern is highly influenced by the stiffness of the supporting soil. For medium-dense and dense sands, the contact pressure typically exhibits a saucer-shaped distribution. This means that pressure values are higher near the periphery and lower towards the center of the raft. The pressure follows a non uniform but symmetric pattern, reflecting moderate soil flexibility and the raft's ability to deform slightly under the loading. For highly flexible soils (such as loose sands), the contact pressure assumes a bowl-shaped distribution. The maximum pressure occurs at the center or under areas with maximum load (such as the leeward side under wind loading), while the edges experience less pressure. This pattern indicates greater soil deformation, and the raft essentially sinks more deeply under the concentrated loads. Specifically, along-loading: On the windward side, the contact pressure varies linearly, due to uplift tendencies and reduced soil contact. On the leeward side: For flexible soils, the maximum pressure occurs uniformly across a larger area. For stiffer soils, the maximum contact pressure is concentrated at the innermost edge of the raft, forming a more defined bowl shape. This variation in contact pressure distribution demonstrates that the actual foundation behavior under wind loads is significantly influenced by soil flexibility and underscores the importance of including SSI effects in the structural analysis and design of tall chimneys and similar structures.

Fig. 9 illustrates the contact pressure distribution beneath the raft of the chimney having a slenderness ratio, H/D<sub>b</sub>=7 and outer diameter of raft to its thickness ratio,  $D_0/t=12.5$ under along-wind loading. The observed pattern of contact pressure takes the form of a shallow bowl, which is a characteristic of flexible foundations resting on deformable soil. In softer soils, the contact pressure is more uniformly spread but with lower intensity, due to the higher deformability and lower stiffness of the supporting medium. As the soil becomes denser (i.e., transitions from loose to medium dense, dense, and very dense conditions), the contact pressure beneath the raft increases significantly. This is because stiffer soils resist deformation more effectively, resulting in higher reactive pressures under the same loading conditions. The bowl-shaped distribution indicates that the maximum contact pressure typically occurs towards the central region of the raft (near the windshield), while lower pressures appear towards the outer edges. This behavior confirms that soil stiffness plays a vital role in the transmission and distribution of loads from the superstructure to the foundation. The findings from Fig. 6 emphasize the necessity of including SSI effects in the design of tall structures like chimneys, particularly to ensure safety and optimized foundation performance under lateral wind-induced loads.

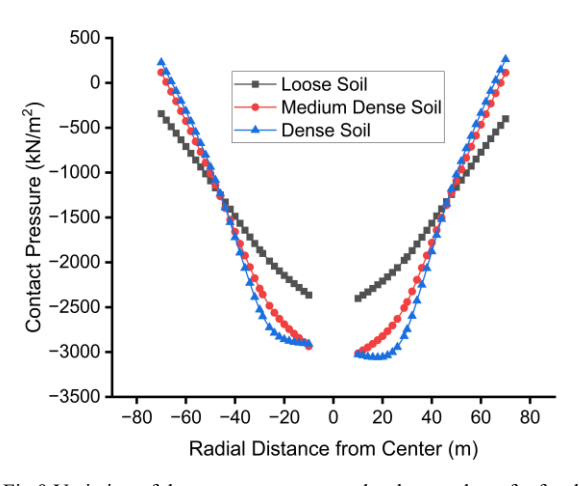


Fig. 9 Variation of the contact pressure under the annular raft of a chimney with  $H/D_b=7$  and ratio  $D_0/t$  =12.5

Fig. 10 illustrates the contact pressure distribution beneath the raft of a chimney with a slenderness ratio,  $H/D_b=12$  and outer diameter of raft to its thickness ratio,  $D_0/t=12.5$  under along-wind loading. The observed contact pressure pattern closely mirrors the vertical displacement trend presented in Fig. 4. Similarly, Fig. 11 depicts a contact pressure distribution that corresponds to the vertical displacement pattern shown in Fig. 5. It is observed that the contact pressure beneath the raft decreases for chimneys with slenderness ratios of 12 and 17 when compared to that of a chimney with a slenderness ratio of 7. This reduction is

attributed to the increased flexibility and load dispersion of taller chimney structures.

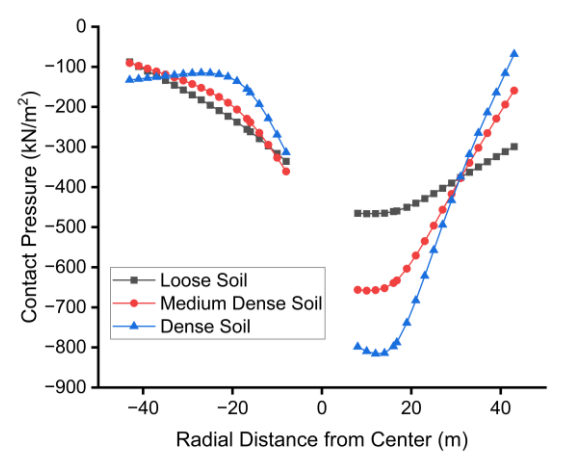


Fig. 10 Variation of the contact pressure under the annular raft of a chimney with  $H/D_b=12$  and  $D_0/t=12.5$ 

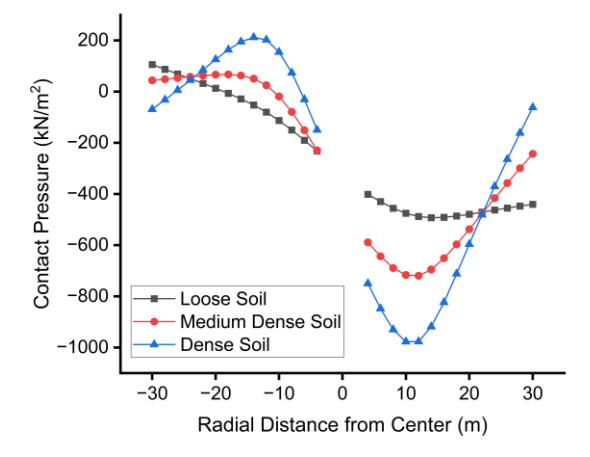


Fig.11 Variation of the contact pressure under the annular raft of a chimney with  $H/D_b=17$  and  $D_0/t=12.5$ 

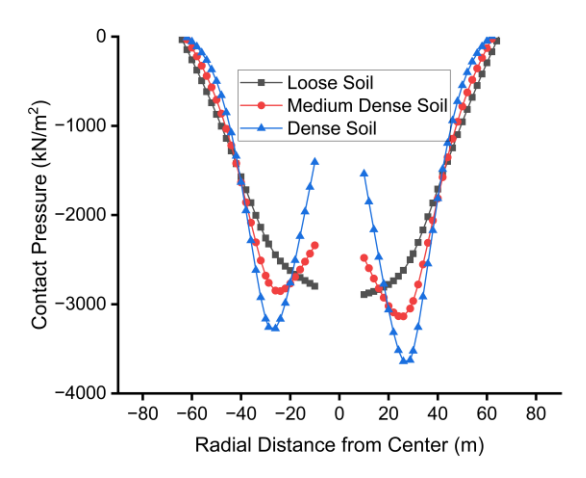


Fig.12 Variation of the contact pressure under the annular raft of a chimney with  $H/D_b=7$  and  $D_0/t=22.5$ 

Fig. 12 depicts the contact pressure distribution beneath the raft foundation for  $D_0/t$  ratio of 22.5. In comparison with Fig. 9, which corresponds to a  $D_0/t$  ratio of 12.5, reveals that the contact pressure in Fig. 12 is approximately 26.3% higher across all soil types. This increase is directly attributed to the reduction in raft thickness associated with higher  $D_0/t$  ratio. A thinner raft offers reduced flexural rigidity, which leads to a greater load concentration and,

consequently, higher contact stresses being transferred to the supporting soil. A similar trend is observed in Fig. 13 and 14, where the contact pressure values are 34.14% higher compared to Fig. 10 and 11, respectively.

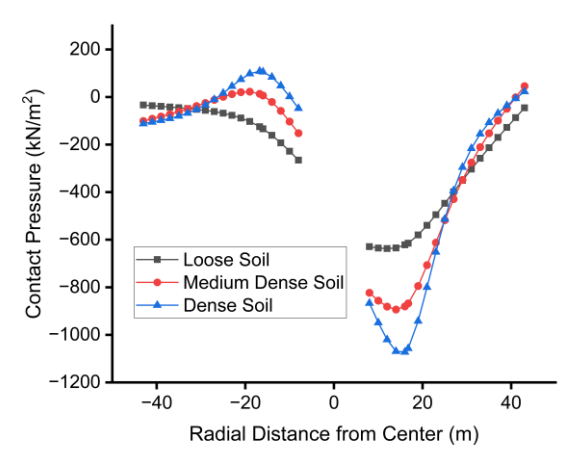


Fig.13 Variation of the contact pressure under the annular raft of a chimney with  $H/D_b$ =12 and  $D_0/t$  =22.5

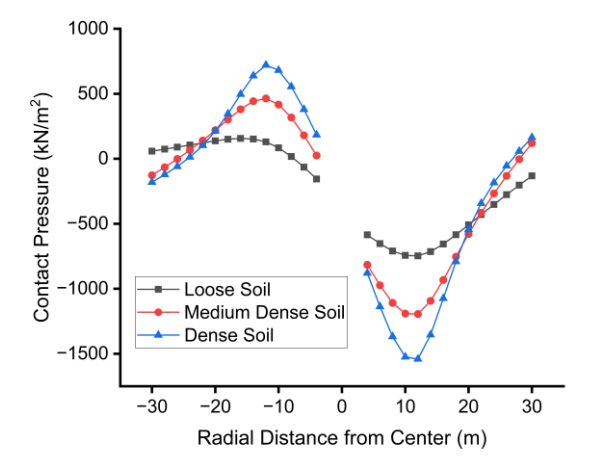


Fig.14 Variation of the contact pressure under the annular raft of a chimney with  $H/D_b=17$  and  $D_0/t$  =22.5

# C. Variation of the tangential moments in a Chimney raft

It is observed that the variation pattern of tangential bending moments obtained from SSI analysis generally follows the same overall trend as that predicted by the conventional method. However, there is a notable difference in the location and magnitude of the maximum moments between the two approaches. In the conventional method, which assumes a rigid foundation with uniform contact pressure, the maximum tangential moment typically occurs at the innermost radius of the raft. This is due to the assumption that the entire raft behaves as a single stiff body, and the curvature and hence bending is most pronounced at the inner edge. In contrast, the SSI method, which accounts for soil flexibility and actual pressure distribution, reveals that the maximum tangential moments shift in location and increase in magnitude. Specifically, the maximum moment is observed near the windshield location, where the leeward side of the raft experiences the greatest differential settlement and contact pressure due to the applied wind load. The increased flexibility of the soil under the leeward side allows more rotation and curvature in the raft, resulting in higher bending moments at that specific zone. This shift in moment location from the innermost edge in conventional analysis to the wind-loaded leeward side in SSI analysis highlights the importance of capturing the realistic soil response and foundation behavior under dynamic lateral loading.

Fig. 15 illustrates the variation of tangential moments in the raft of a chimney with a slenderness ratio, H/D<sub>b</sub>=7 and outer diameter of raft to its thickness ratio, D<sub>0</sub>/t=12.5 under different subsoil conditions. It is observed that as the K<sub>s</sub> of the soil increases, the tangential moment in the raft decreases. Using the Elastic Continuum method, the tangential moment for loose soil conditions shows a reduction of 21.97% compared to the conventional IS code based method. For medium-dense and dense soil, the reductions are more pronounced at 67.32% and 80.37%, respectively. This trend highlights the effectiveness of the Elastic Continuum model in capturing soil-structure interaction more accurately than conventional methods. In contrast, the Winkler Spring method also shows a decrease in tangential moments with increasing soil stiffness, but the percentage reduction is comparatively lower than that obtained through the Elastic Continuum approach.

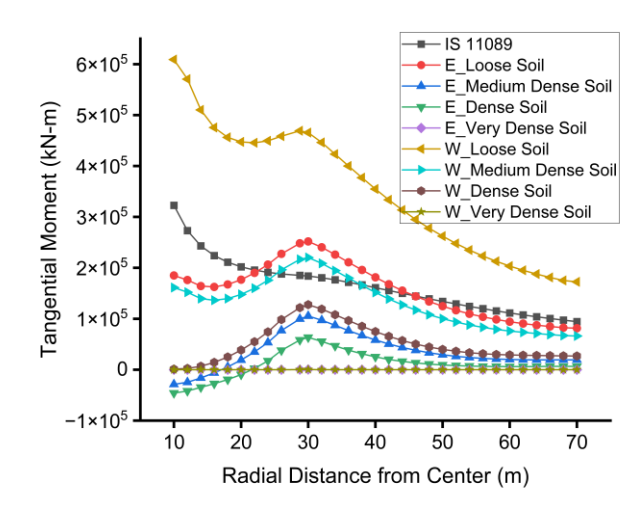


Fig.15 Variation of tangential moments in an annular raft of a chimney with  $H/D_b{=}7$  and  $D_0/t$  =12.5

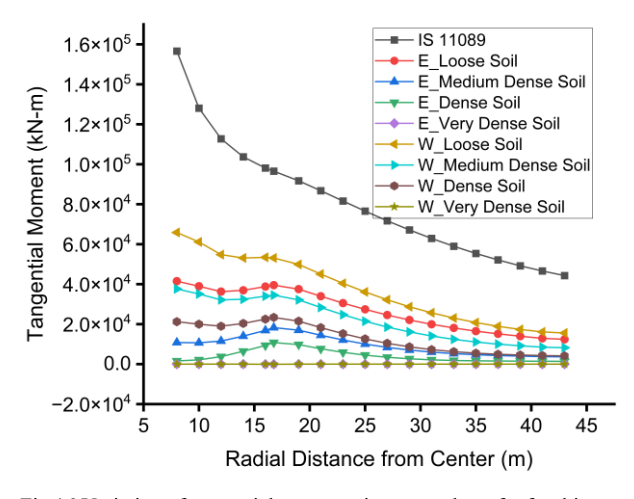


Fig.16 Variation of tangential moments in an annular raft of a chimney with  $H/D_b{=}12$  and  $D_0/t$  =12.5

Fig. 16 illustrates the variation of tangential moments in the raft of a chimney with a slenderness ratio,  $H/D_b=12$  and

outer diameter of raft to its thickness ratio, D<sub>0</sub>/t=12.5 under different subsoil conditions for a chimney with a higher slenderness ratio. It is observed that as the subgrade modulus of the soil increases, the tangential moment in the raft decreases. Compared to the chimney with a slenderness ratio of 7, the reduction in tangential moments is more significant for each soil type in this configuration when analyzed using the Elastic Continuum method. This indicates that taller chimneys exhibit greater sensitivity to subsoil stiffness in terms of tangential moment reduction. In contrast, the Winkler Spring method also shows a decreasing trend with increasing soil stiffness, but the percentage reductions are consistently lower than those obtained from the Elastic Continuum model, highlighting the latter's ability to more accurately reflect soil-structure interaction effects.

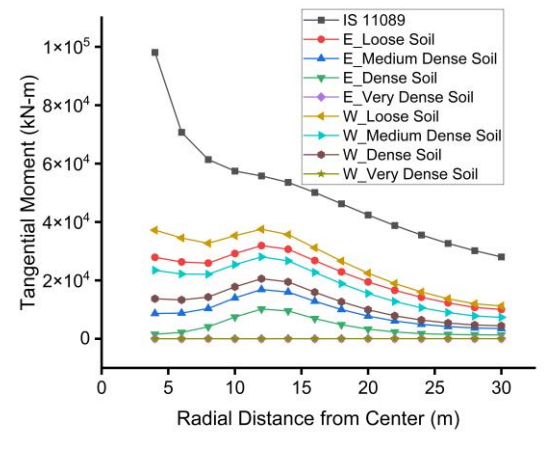


Fig.17 Variation of tangential moments in an annular raft of a chimney with  $H/D_b$ =17 and  $D_0/t$ =12.5

Fig. 17 depicts the tangential moments in the raft of a chimney with a slenderness ratio, H/D<sub>b</sub>=17 and outer diameter of raft to its thickness ratio, D<sub>0</sub>/t=12.5 under different subsoil conditions. When using the Elastic Continuum method, the reduction in tangential moments is observed to be less pronounced compared to the chimney with a slenderness ratio of 12, indicating that the effectiveness of increased soil stiffness in reducing moments diminishes at higher slenderness ratios. Conversely, the Winkler Spring method shows a greater percentage decrease in tangential moments for the chimney with slenderness ratio H/D<sub>b</sub>=17 than for chimneys of both H/D<sub>b</sub>=7 and H/D<sub>b</sub>=12. This suggests that the Winkler Spring model, though more simplified, may exhibit enhanced sensitivity to soil stiffness in slender chimneys, potentially due to the distribution characteristics of subgrade reactions in the model.

Fig. 18, 19, and 20 present the variation of tangential moments in the annular raft. When compared to Fig 15, 16, and 17, it is evident here that the tangential moments are significantly lower across all soil types. This reduction can be attributed to the increase in  $D_0/t$  ratio, which results in a considerable decrease in raft thickness. A thinner raft possesses lower flexural stiffness, causing it to behave more like a flexible raft rather than a rigid one. In such cases, the raft undergoes greater deformation subjected to loading, thereby reducing the magnitude of tangential moments but potentially increasing overall deflections.

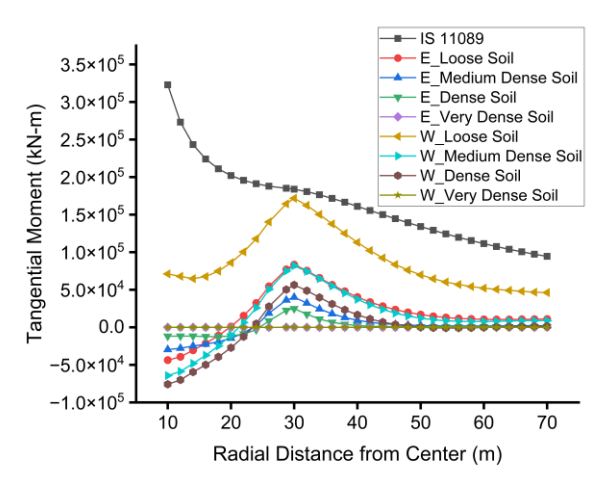


Fig.18 Variation of tangential moments in an annular raft of a chimney with  $H/D_{\,b}{=}7$  and  $D_{\,0}/t$  =22.5

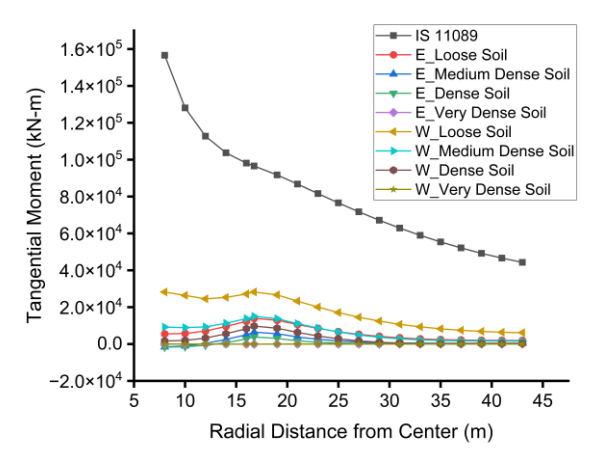


Fig.19 Variation of tangential moments in an annular raft of a chimney with  $H/D_b\!=\!12$  and  $D_0/t$  =22.5

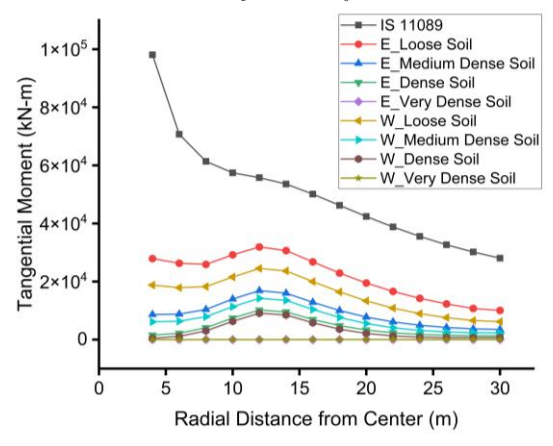


Fig.20 Variation of tangential moments in an annular raft of a chimney with  $H/D_b\!=\!17$  and  $D_0/t$  =22.5

# D. Variation of the radial moments in a Chimney raft

It is observed that the radial bending moment patterns derived from both SSI methods, the Winkler Spring model and the Elastic Continuum, are consistent with those obtained from the conventional method in terms of an overall trend. In all cases, the maximum radial moments occur on the leeward side of the chimney, which is subjected to higher loads due to wind-induced pressures. However, a key difference lies in the magnitude of the radial moments, which is significantly influenced by the flexibility of the supporting soil. As the soil flexibility decreases, the radial

moments reduce in magnitude. This behavior occurs because rigid soils provide stronger support, limiting differential settlement and reducing bending in the foundation. In such cases, the raft behaves more like a flexible plate resting on a stiff medium, distributing loads more evenly and reducing peak moment values. In contrast, when the soil is more flexible, the foundation undergoes greater differential settlements, which lead to higher radial moments, particularly on the leeward side where uplift is minimal and downward displacement is maximum. Thus, while the shape and pattern of radial moment distribution remain similar across all methods, the soil stiffness directly affects the intensity of these moments.

Fig. 21 illustrates the variation of radial moments in the raft foundation for a chimney with a slenderness ratio,  $H/D_b=7$  and outer diameter of raft to its thickness ratio,  $D_0/t=12.5$ . It is observed that as the  $K_s$  increase, the radial moments decrease, indicating improved support conditions and reduced bending demand on the raft. However, when comparing the results to those obtained using the conventional IS code method, the radial moments predicted by both Elastic Continuum and Winkler Spring methods are higher. This suggests that the simplified assumptions in the IS code may underestimate the actual moment demand, whereas the more refined soil-structure interaction models (Elastic and Winkler) provide a more realistic, though conservative, estimate of the radial moment behavior.

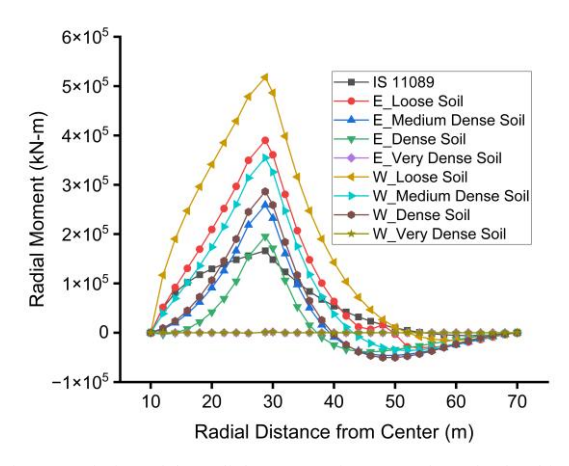


Fig.21 Variation of the radial moments in an annular raft of a chimney with  $\rm H/D_b{=}7$  and  $\rm D_0/t$  =12.5

Fig. 22 illustrates the variation of radial moments in the raft foundation for a chimney with a slenderness ratio, H/D<sub>b</sub>=12 and outer diameter of raft to its thickness ratio,  $D_0/t=12.5$ . Compared to H/D<sub>b</sub>=7 configuration, the radial moments in this setup are reduced, indicating a more favorable distribution of loads with increased chimney height. When compared to the IS code method, both the Elastic Continuum and Winkler Spring methods show lower radial moment values, suggesting that conventional code based estimates may be conservative for taller chimneys. Furthermore, the Elastic Continuum method exhibits a greater reduction in radial moments than the Winkler Spring method. Fig. 23 describes a similar pattern of radial moment variation as observed in Fig. 22 for a chimney with a slenderness ratio of H/D<sub>b</sub>=12. In general, radial moments decrease with increasing soil stiffness across all methods. However, it is noteworthy that for loose soil conditions, the radial moments obtained using both the Elastic Continuum and Winkler Spring methods are higher than those estimated by the IS code method, indicating a possible underestimation by the conventional approach in less stiff soils. For medium and dense soils, the IS code method overestimates the radial moments when compared to the analytical models, aligning with trends observed in lower slenderness ratio configurations.

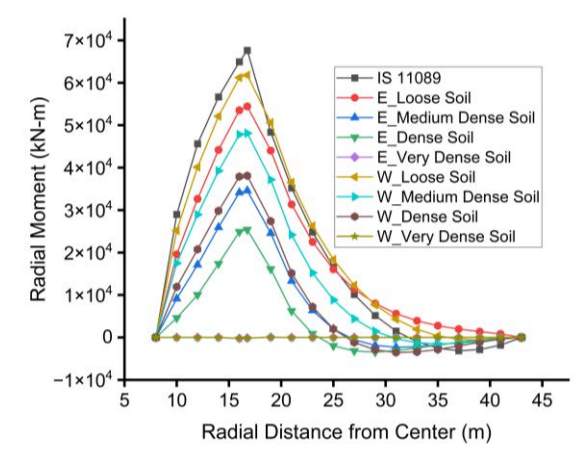


Fig.22 Variation of the radial moments in an annular raft of a chimney with  $H/D_b{=}12$  and  $D_0/t$  =12.5

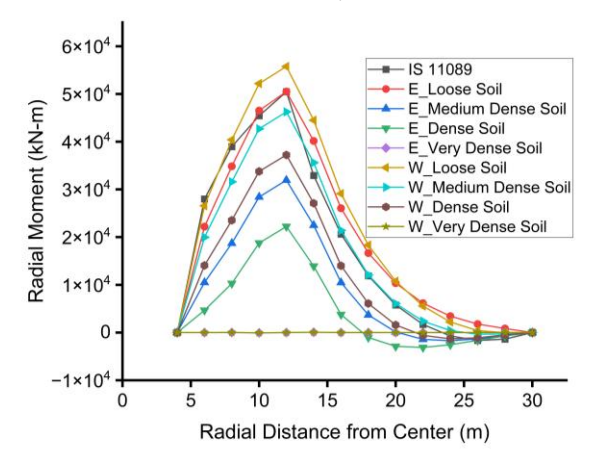


Fig.23 Variation of the radial moments in an annular raft of a chimney with  $\rm H/D_b{=}17$  and  $\rm D_0/t$  =12.5

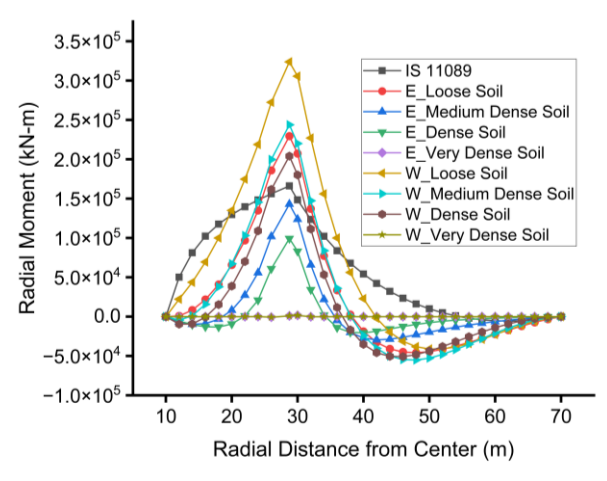


Fig.24 Variation of the radial moments in an annular raft of a chimney with  $\rm H/D_b{=}7$  and  $\rm D_0/t$  =22.5

Fig. 24, 25, and 26 illustrate the variation of radial moments in the annular raft. Compared to Fig. 21, 22, and 23, the radial moments are noticeably lower across all soil types. This reduction is primarily due to an increase in the

 $D_0/t$  ratio, which leads to a decrease in raft thickness. A thinner raft exhibits reduced flexural stiffness, causing it to behave more like a flexible raft rather than a rigid one. Consequently, the raft experiences greater deformation under loading, which lowers the magnitude of radial moments like tangential moments.

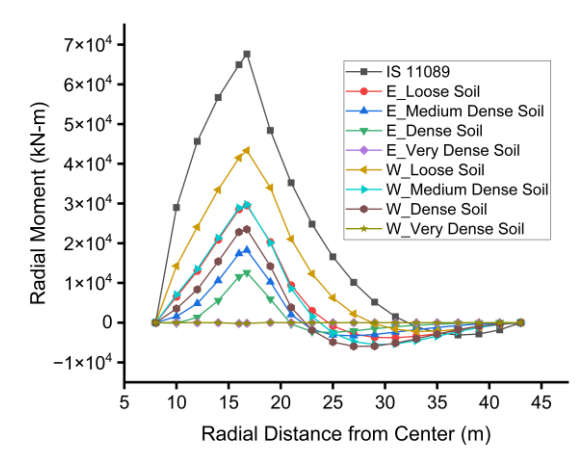


Fig.25 Variation of the radial moments in an annular raft of a chimney with  $\rm H/D_b{=}12$  and  $\rm D_0/t$  =22.5

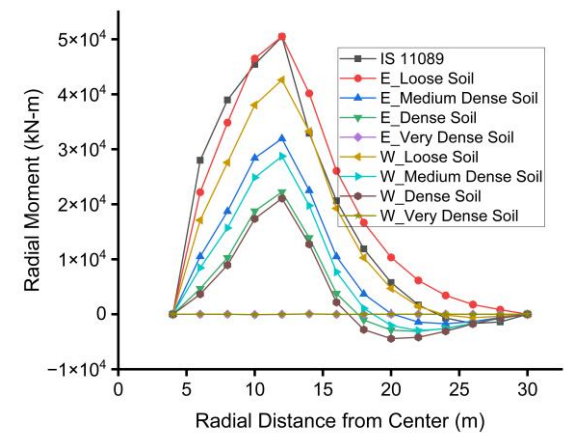


Fig.26 Variation of the radial moments in an annular raft of a chimney with  $H/D_b\!=\!17$  and  $D_0/t$  =22.5

# E. Variation of the natural frequency in a chimney

Reinforced concrete chimney shafts, owing to their tall, slender, and axisymmetric configuration, exhibit significant stiffness. However, when such structures rest on an RCC raft foundation supported by soil, the effect of SSI becomes an important factor in evaluating their dynamic response. Unlike an idealized fixed-base condition, where the base is assumed to be perfectly rigid, the actual interaction between the chimney and its supporting soil introduces flexibility into the system. This interaction alters the dynamic characteristics of the structure, most notably by increasing its fundamental period. In other words, the coupling between the structure and the deformable soil generally leads to a system that responds more slowly to dynamic excitations, such as wind or seismic forces, compared to the same structure modeled on a rigid base. This elongation of the fundamental period is a direct consequence of the reduced stiffness of the overall system due to soil compliance.

TABLE IV VARIATION OF NATURAL FREQUENCIES IN CHIMNEY FOR DIFFERENT H/  $D_{\scriptscriptstyle B}$  RATIO

| Soil Type      | Mode no. | I I       | Frequency (Hz)       |          |  |  |
|----------------|----------|-----------|----------------------|----------|--|--|
|                |          | $H/D_b=7$ | $H/D_b=12$ $H/D_b=1$ |          |  |  |
| Fixed base (IS | 1        | 0.64      | 0.2                  | 0.13     |  |  |
| 11089)         | 2        | 2.15      | 0.82                 | 0.6      |  |  |
|                | 3        | 3.5       | 1.8                  | 1.46     |  |  |
|                | 4        | 3.99      | 1.81                 | 2.45     |  |  |
|                | 5        | 5.43      | 1.92                 | 2.58     |  |  |
| E_ Loose Soil  | 1        | 1.00E-04  | 8.60E-05             | 3.70E-04 |  |  |
|                | 2        | 1.10E-04  | 9.70E-05             | 4.10E-04 |  |  |
|                | 3        | 1.30E-04  | 1.00E-04             | 4.60E-04 |  |  |
|                | 4        | 1.50E-04  | 1.20E-04             | 5.30E-04 |  |  |
|                | 5        | 1.50E-04  | 1.40E-04             | 6.0E-04  |  |  |
| E_ Medium      | 1        | 2.00E-04  | 1.70E-04             | 7.40E-04 |  |  |
| Dense Soil     | 2        | 2.20E-04  | 1.90E-04             | 8.30E-04 |  |  |
|                | 3        | 2.60E-04  | 2.10E-04             | 9.30E-04 |  |  |
|                | 4        | 3.00E-04  | 2.50E-04             | 1.00E-03 |  |  |
|                | 5        | 3.0E-04   | 2.80E-04             | 1.20E-03 |  |  |
| E_ Dense Soil  | 1        | 3.10E-04  | 2.70E-04             | 1.10E-03 |  |  |
|                | 2        | 3.60E-04  | 3.00E-04             | 1.30E-03 |  |  |
|                | 3        | 4.10E-04  | 3.40E-04             | 1.40E-03 |  |  |
|                | 4        | 4.70E-04  | 3.90E-04             | 1.70E-03 |  |  |
|                | 5        | 4.80E-04  | 4.40E-04             | 1.90E-03 |  |  |
| E_ Very Dense  | 1        | 0.18      | 0.2                  | 0.14     |  |  |
| Soil           | 2        | 0.61      | 0.83                 | 0.6      |  |  |
|                | 3        | 1.0       | 1.83                 | 1.48     |  |  |
|                | 4        | 1.14      | 1.84                 | 2.48     |  |  |
|                | 5        | 1.56      | 1.95                 | 2.62     |  |  |
| W_ Loose Soil  | 1        | 0.14      | 0.18                 | 0.12     |  |  |
|                | 2        | 0.6       | 0.76                 | 0.55     |  |  |
|                | 3        | 0.77      | 1.82                 | 1.36     |  |  |
|                | 4        | 1.14      | 1.83                 | 2.31     |  |  |
|                | 5        | 1.56      | 1.84                 | 2.48     |  |  |
| W_ Medium      | 1        | 0.16      | 0.19                 | 0.13     |  |  |
| Dense Soil     | 2        | 0.61      | 0.79                 | 0.58     |  |  |
|                | 3        | 0.91      | 1.83                 | 1.41     |  |  |
|                | 4        | 1.14      | 1.84                 | 2.48     |  |  |
|                | 5        | 1.56      | 1.89                 | 2.6      |  |  |
| W_ Dense Soil  | 1        | 0.17      | 0.19                 | 0.13     |  |  |
|                | 2        | 0.61      | 0.8                  | 0.58     |  |  |
|                | 3        | 0.96      | 1.83                 | 1.43     |  |  |
|                | 4        | 1.14      | 1.84                 | 2.48     |  |  |
|                | 5        | 1.56      | 1.91                 | 2.61     |  |  |
| W_ Very Dense  | 1        | 0.18      | 0.2                  | 0.14     |  |  |
| Soil           | 2        | 0.61      | 0.83                 | 0.6      |  |  |
|                | 3        | 1         | 1.83                 | 1.48     |  |  |
|                | 4        | 1.14      | 1.84                 | 2.48     |  |  |
|                |          |           |                      |          |  |  |

| 5 | 1.56 | 1.95 | 2.62 |
|---|------|------|------|

Analysis of the results presented in Table IV reveals a clear influence of soil flexibility on the natural frequency of reinforced concrete chimneys, particularly when different analytical methods and soil conditions are considered. When using the Elastic Continuum approach, there is a dramatic reduction in the natural frequency across all soil types: 99.9% for loose soil, 99.8% for medium dense soil, and 99.7% for dense soil when compared to the fixed-base scenario. This significant drop highlights the pronounced effect of soil compliance in this method, which accounts for the continuous deformation of the soil mass beneath the structure. In contrast, the Winkler foundation model, which idealizes the soil as a system of discrete, independent springs, shows a less severe reduction in natural frequencies. For the same soil conditions, the reductions are 25% for loose soil, 11% for medium dense soil, and 6.3% for dense soil. These comparatively modest changes reflect the simplified nature of the Winkler Spring model, which may underestimate the broader deformation behavior of the supporting soil mass. Furthermore, it is observed that for very dense soil, both the Elastic Continuum and Winkler Spring methods yield natural frequencies that are virtually identical to those of the fixed-base condition. This outcome is attributed to the high stiffness of the very dense soil, which behaves almost like a rigid base, thereby minimizing the effects of soil-structure interaction regardless of the slenderness ratio of the chimney.

Fig. 27 clearly illustrates that the fundamental natural frequency of the chimney decreases as the slenderness ratio increases. This trend indicates that taller chimneys exhibit greater structural flexibility, making them more sensitive to dynamic effects such as wind or seismic loading. This reduction in frequency is consistently observed across all types of supporting soil, emphasizing the combined influence of geometric slenderness and soil compliance on the dynamic behavior of the structure. Furthermore, when evaluating the system using the elastic continuum approach, the natural frequency tends to approach near-zero values. This is primarily attributed to the significant flexibility introduced by the surrounding soil in this method, which models the soil as a continuous, deformable medium. The resulting interaction between the flexible soil and the tall, slender chimney significantly reduces the system's stiffness, thereby lowering its natural frequency to very small values. In contrast, the Winkler Spring model, which represents the soil as a series of independent, discrete springs, produces natural frequency of non-zero. However, even in this case, the frequency remains lower than that of the idealized fixed base model. This indicates that while the Winkler Spring method accounts for soil flexibility to a certain extent, it offers a more simplified and moderate representation compared to the elastic continuum model.

# IV. CONCLUSIONS

A tall chimney model with three different slenderness ratios of chimney (H/D<sub>b</sub>=7, 12, and 17) and two different outer diameter to thickness ratios of raft (D<sub>0</sub>/t=12.5 and 22.5) was analyzed under the influence of along-wind loading, considering two distinct SSI modeling approaches:

the Winkler Spring model and the Elastic Continuum model. The study focused on evaluating critical structural responses, including the vertical displacement of the annular raft, contact pressure beneath the raft, tangential moments, and radial moments. Based on the comprehensive analysis of the results, the following key conclusions are drawn:

- The vertical displacement of the annular raft exhibits a clear inverse relationship with the modulus of subgrade reaction of the supporting soil. As the soil stiffness increases, the vertical displacement of the raft significantly decreases, reflecting the enhanced resistance provided by stiffer soils. A detailed examination of the displacement pattern reveals that the maximum vertical displacement consistently occurs at the windshield location on the leeward side of the annular raft. This behavior is attributed to the asymmetrical loading effects induced by the along-wind force acting on the chimney structure. On the leeward side, the wind creates a compressive force, resulting in a downward deformation of the raft beneath that region. Conversely, the windward side experiences tensional effects, leading to a relatively lower downward displacement or even a slight uplift, depending on the flexibility of the supporting soil.
- 2) The contact pressure beneath the annular raft shows a decreasing trend with the increasing slenderness ratio of the chimney. This behavior is primarily attributed to the reduction in raft diameter associated with taller, more slender chimneys. As the slenderness ratio (H/D<sub>b</sub>) increases, the effective area over which the load is distributed decreases, and the raft tends to behave more like a rigid plate resting on a relatively flexible soil medium. This rigidity causes a more uniform but lower overall contact pressure, especially for chimneys with higher slenderness.
- With the increase in outer diameter to thickness ratio of the raft, the load concentration and so the pressure exerted by a chimney shell on the raft increases. This leads to increased vertical displacement and non uniform stress distribution in the foundation system with higher peaks which may even cause larger differential settlement. Rotation under overturning increases, magnifying differential compression/tension in the soil. A thinner raft because of higher D0/t offers reduced flexural rigidity, which leads to a greater load concentration and, consequently, higher contact stresses being transferred to the supporting soil. A thinner raft exhibits reduced flexural stiffness, causing it to behave like a flexible raft rather than rigid. Consequently, the raft experiences greater deformation underloading, which reduces the magnitude of radial and tangential moments.
- 4) As the modulus of the subgrade reaction increases, indicating a stiffer supporting soil, the contact pressure beneath the raft increases. This increase occurs because of more flexible behavior when placed on rigid soil, leading to non-uniform pressure distribution with higher intensity values, particularly near critical locations such as the leeward edge.
- 5) The tangential and radial moments observed in the annular raft exhibit a clear trend in relation to the

- modulus of the subgrade reaction of the soil. Specifically, as the  $K_s$  value increases, indicating a stiffer soil medium, the tangential and radial moments in the raft decrease. This reduction can be attributed to the improved load-distribution characteristics provided by the stiffer soil, which better supports the raft and reduces bending effects.
- 6) When the results from the Soil-Structure Interaction analysis are compared with those obtained using the conventional method (which typically assumes a rigid foundation and uniform pressure distribution), it is evident that the SSI approach predicts lower tangential and radial moments. This is because SSI modeling captures the actual interaction between the soil and structure, leading to a more realistic and less conservative estimation of internal forces.
- 7) The Elastic Continuum method results in the lowest tangential and radial moments, reflecting its ability to simulate a more continuous and distributed soil response. The Winkler spring model, while also

- predicting lower moments than the conventional method, shows higher tangential and radial moments than the Elastic Continuum model, as it simplifies the soil behavior using discrete springs without capturing the continuous interaction across the foundation.
- 8) As the flexibility of the supporting soil increases, there is a noticeable decrease in the natural frequency of the structure. This inverse relationship highlights the fundamental influence of SSI on the dynamic behavior of structural systems.
- 9) In a flexible soil environment, the foundation experiences greater deformation under dynamic loads, which effectively reduces the overall stiffness of the soil-structure system. This reduction in stiffness leads to an elongation of the natural period and, consequently, a lowering of the natural frequency. Such changes in dynamic characteristics are crucial in structural design and wind analysis, as they can significantly alter the response of the structure to vibrational forces.

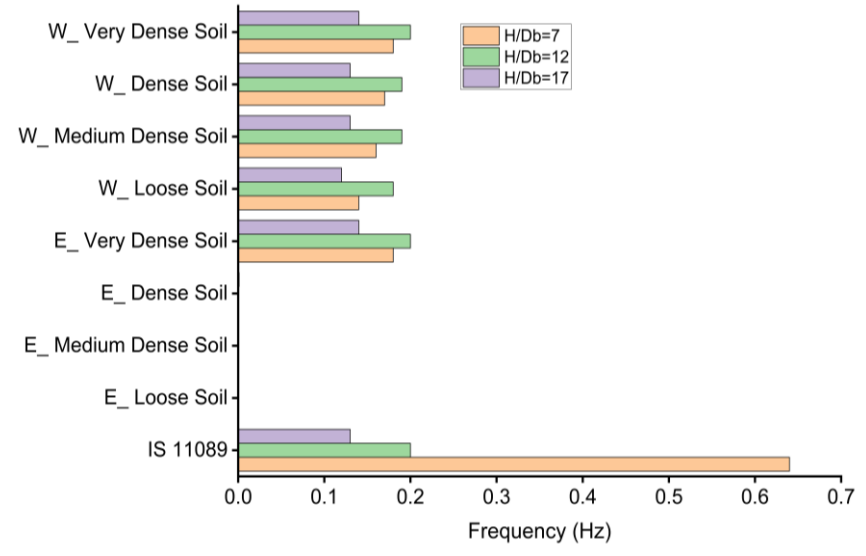


Fig.27 Variation of the natural frequency in a chimney

# $\label{table I} \textbf{TABLE I}$ Geometrical Properties of the chimney shell and annular raft

| Diameter<br>at base<br>D <sub>b</sub> in (m) | Slenderness<br>ratio<br>H/D <sub>b</sub> | Taper ratio $D_t/D_b$ | Diameter at top $D_t$ in (m) | Thickness at the base $T_b$ in (m) | Thickness at top $T_t = 0.4$ $T_b$ or $0.2m$ | Raft external diameter D <sub>o</sub> in (m) | Raft internal diameter D <sub>i</sub> in (m) | Raft Outer<br>diameter to Raft<br>thickness (t) ratio<br>$D_o/t$ |      |
|--|--|-----------------------|------------------------------|------------------------------------|--|--|--|--|------|
|  |  |                       |                              |                                    |  |  |  | 12.5   | 22.5 |
| 57.5   | 7  | 0.6                   | 34.5                         | 1.7                                | 0.7  | 140.0  | 20.0   | 11.2   | 6.30 |
| 33.5   | 12                                       | 0.6                   | 20.1                         | 1.0                                | 0.4  | 86.0   | 16.0   | 6.88   | 3.90 |
| 24.0   | 17                                       | 0.6                   | 14.4                         | 0.7                                | 0.3  | 60.0   | 8.0  | 4.80   | 2.70 |

#### REFERENCES

- [1] L. P. Correia, S. Rafael, S. Sorte, V. Rodrigues, C. Borrego, and A. Monteiro, "High-resolution analysis of wind flow behavior on ship stacks configuration: A Portuguese case study," *Atmosphere (Basel).*, vol. 12, no. 3, 2021, doi: 10.3390/atmos12030303.
- [2] M. Lungu and N. Stefu, "Study on particulate matter dispersion by correlating direct measurements with numerical simulations: Case study—Timisoara urban area," *Int. J. Environ. Sci. Technol.*, vol. 15, no. 7, 2018, doi: 10.1007/s13762-017-1521-x.
- [3] A. S. Mathew and R. P. Mohan, "Analysis of tall chimney with piled raft foundation under wind load using ANSYS," *IOP Conf. Ser. Mater. Sci. Eng.*, vol. 1114, no. 1, 2021, doi: 10.1088/1757-899x/1114/1/012017.
- [4] M. Yamamoto and C. J. Ma, "Development of a model instrument of thermal power plant for understanding of air pollutant generation," *Asian J. Atmos. Environ.*, vol. 10, no. 3, 2016, doi: 10.5572/ajae.2016.10.3.156.
- [5] F. Zair, M. Mouqallid, and E. H. Chatri, "Numerical simulation of pollutants dispersion emitted by a bent chimney," *Environ. Fluid Mech.*, vol. 22, no. 1, 2022, doi: 10.1007/s10652-022-09833-w.
- [6] P. Nealipuri, M. N. Pradhan, H. C. Das, R. N. Mahapatra, and B. Das, "Prediction of Air Pollutants Emitting from Chimney of A CHP Using CFD," *Internatioal J. Sci. Eng. Res.*, vol. 9, no. 4, 2018
- [7] F. N. Zai and A. Y. Gunawan, "Effects of inversion layer on the atmospheric pollutant dispersion from a high chimney," J.

- *Indones. Math. Soc.*, vol. 29, no. 3, 2023, doi: 10.22342/jims.29.3.1597.299-310.
- [8] B. R. Jayalekshmi, S. V. Jisha, and R. Shivashankar, "Response in piled raft foundation of tall chimneys under along-wind load incorporating flexibility of soil," *Front. Struct. Civ. Eng.*, vol. 9, no. 3, 2015, doi: 10.1007/s11709-015-0288-8.
- [9] S. V. Jisha, B. R. Jayalekshmi, and R. Shivashankar, "3D soil–structure interaction analyses of annular raft foundation of tall RC chimneys under wind load," *Indian Geotech. J.*, vol. 44, no. 4, 2014, doi: 10.1007/s40098-013-0095-x.
- [10] B. R. Jayalekshmi, S. V. Jisha, and R. Shivashankar, "Soil-Structure Interaction Analysis of Tall Reinforced Concrete Chimney with Piled Raft and Annular Raft under Along-Wind Load," J. Struct., vol. 2013, 2013, doi: 10.1155/2013/859246.
- [11] B. R. Jayalekshmi, S. V. Jisha, and R. Shivashankar, "Response of tall chimneys with piled raft and annular raft foundation under wind loads considering SSI," in Computer Methods and Recent Advances in Geomechanics Proceedings of the 14th Int. Conference of International Association for Computer Methods and Recent Advances in Geomechanics, IACMAG 2014, 2015. doi: 10.1201/b17435-175.
- [12] L. Lakshmi, M. L. Burnwal, S. Ray Chaudhuri, and P. Raychowdhury, "Dynamic response of tall chimneys on pile–raft foundation subjected to wind load," in *Lecture Notes in Civil Engineering*, 2020. doi: 10.1007/978-981-15-6090-3\_38.
- [13] B. R. Jayalekshmi, S. V. Jisha, and R. Shivashankar, "Wind load analysis of tall chimneys with piled raft foundation considering the flexibility of soil," *Int. J. Adv. Struct. Eng.*, vol. 7, no. 2, 2015, doi: 10.1007/s40091-015-0085-6.
- [14] G. S. Sandeep, A. K. Y. M, P. Pandit, and V. B. Alexander, "Effect of Soil-pile Interaction on Inclined Pile Group Subjected to Axial and Lateral Loads," *Eng. Lett.*, vol. 33, no. 7, pp. 2713– 2722, 2025.
- [15] H. N. Raghavendra, P. Kappadi, H. Likhitha, and A. Yadav, "The Behavior of Tapered and Step-Tapered Piles under Lateral Load," Eng. Lett., vol. 33, no. 3, pp. 530–544, 2025.
- [16] S. Elias, V. Matsagar, and T. K. Datta, "Along-wind response control of chimneys with distributed multiple tuned mass dampers," *Struct. Control Heal. Monit.*, vol. 26, no. 1, pp. 1–25, 2019, doi: 10.1002/stc.2275.
- [17] A. K. Gupta, S. S. Bhadauria, and A. Rawat, "Dynamic analysis of RCC chimneys subjected to near-fault ground motions," *Asian J. Civ. Eng.*, vol. 25, no. 3, pp. 2929–2945, 2024, doi: 10.1007/s42107-023-00954-1.
- [18] H. G. Poulos, J. C. Small, and H. Chow, "Piled raft foundations for tall buildings," *Geotech. Eng.*, vol. 42, no. 2, 2011.
- [19] D. Menon and P. S. Rao, "Estimation of along-wind moments in RC chimneys," *Eng. Struct.*, vol. 19, no. 1, 1997, doi: 10.1016/S0141-0296(96)00041-7.
- [20] M. Bhatt and S. Vasanwala, "Comparison of Ultimate Capacities of RC Chimney Sections under Wind Loading," *Trends Sci.*, vol. 19, no. 1, 2022, doi: 10.48048/tis.2022.1722.
- [21] S. A. Naeini, R. Ziaie Moayed, and F. Allahyari, "Subgrade Reaction Modulus (Ks) of Clayey Soils Based on Field Tests," J. Eng. Geol., vol. 8, no. 1, 2014.
- [22] O. Mughieda, M. S. Mehana, and K. Hazirbaba, "Effect of soil subgrade modulus on raft foundation behavior," in MATEC Web of Conferences, 2017. doi: 10.1051/matecconf/201712006010.
- [23] S. Teli, P. Kundhani, V. Choksi, P. Sinha, and K. K. R. Iyer, "Analytical Study on the Influence of Rigidity of Foundation and Modulus of Subgrade Reaction on Behaviour of Raft Foundation," in *Lecture Notes in Civil Engineering*, vol. 56, 2020. doi: 10.1007/978-981-15-0890-5\_16.
- [24] R. Ziaie-Moayed and M. Janbaz, "Effective parameters on modulus of subgrade reaction in clayey soils," *J. Appl. Sci.*, vol. 9, no. 22, 2009, doi: 10.3923/jas.2009.4006.4012.
- [25] K. Rahgooy, A. Bahmanpour, M. Derakhshandi, and A. Bagherzadeh-Khalkhali, "Distribution of elastoplastic modulus of subgrade reaction for analysis of raft foundations," *Geomech. Eng.*, vol. 28, no. 1, 2022, doi: 10.12989/gae.2021.28.1.089.
- [26] Kim Chi-kyung, "Application of Coupling of the Finite Element method with the Boundary Element Solution to Structure in Elastic Solid Continum," *J. Risk Manag.*, vol. 18, no. 1, 2007, doi: 10.21480/tjrm.18.1.200706.002.
- [27] Bureau of Indian Standards, "IS 4998: 2015 Design of Reinforced Concrete Chimneys," vol. 67, no. 10, pp. 788–801, 1970.
- [28] Bureau of Indian Standards, "IS 875 (Part 3): 2015 Design Loads (other Than Earthquake) For Buildings and Structures — Code of Practice Part 3 Wind Loads (Third Revision)," vol. 875, no. 2, pp. 2015–2017, 2020.

- [29] Ansys Inc., "SHELL163 Element Description," *User's Man.*, 2017.
- [30] K. N. Kadam and N. S. Khan, "Buckling Analysis of Thin Walled Cylinders Subjected to Axially Compressive Load by ANSYS," *Int. J. Eng. Res. Technol.*, vol. 2, no. 12, 2013.
- [31] C. G. Wang, X. W. Du, and Z. M. Wan, "Non-linear buckling finite element analysis of membrane wrinkling," *Jisuan Lixue Xuebao/Chinese J. Comput. Mech.*, vol. 24, no. 3, 2007.
- [32] T. Subramani and A. Sugathan, "Finite Element Analysis of Thin Walled-Shell Structures by ANSYS and LS-DYNA," *Int. J. Mod. Eng. Res. www.ijmer.com*, vol. 2, no. 4, 2012.
- [33] R. Al-Sherif and M. A. Ismael, "Structural Performance of Semi-Rigid Connection Steel Frames," *Diyala J. Eng. Sci.*, 2022, doi: 10.24237/dies.2022.15207.
- [34] C. Hao, J. Luo, B. Wang, X. Zhang, and L. Gan, "Causes of Stiffness Degradation in Steel–UHPC Composite Beam-Bolted Connections," *Buildings*, vol. 13, no. 8, 2023, doi: 10.3390/buildings13082064.
- [35] B. Bai and J. Guo, "Finite Element Damping Simulation of Viscous Damper for Simply Supported Beam Vibration Mitigation," in *IOP Conference Series: Earth and Environmental* Science, 2020. doi: 10.1088/1755-1315/525/1/012162.
- [36] R. B. Hafiz, S. Ahmed, S. Barua, and S. R. Chowdhury, "Effects of Opening on the Behavior of Reinforced Concrete Beam," *IOSR J. Mech. Civ. Eng.*, vol. 11, no. 2, 2014, doi: 10.9790/1684-11275261
- [37] S. Taufik, E. Anggarini, and I. Setiawan, "ANSYS Numerical Modeling of Confined Deep Beam with High Strength Concrete," *Int. J. Struct. Glas. Adv. Mater. Res.*, vol. 4, no. 1, 2020, doi: 10.3844/sgamrsp.2020.41.55.